

A Monte Carlo method to estimate cell population heterogeneity

Ben Lambert^{1,2*}, David J. Gavaghan³, Simon Tavener⁴.

1 Department of Zoology, University of Oxford, Oxford, Oxfordshire, U.K.

2 MRC Centre for Global Infectious Disease Analysis, School of Public Health, Imperial College London, London W2 1PG, UK.

3 Department of Computer Science, University of Oxford, Oxford, U.K.

4 Department of Mathematics, Colorado State University, Fort Collins, Colorado, U.S.A.

*ben.c.lambert@gmail.com.

Revision date & time: 2019-05-25 19:15

1 Abstract

1
2
3
4
5
6
7
8
9
10
11
12
13
14
15
16
17
18
19
20
21
22
23
24
25
26

Variation is characteristic of all living systems. Laboratory techniques such as flow cytometry can probe individual cells and, after decades of experimentation, it is clear that even members of seemingly homogeneous cell populations can exhibit differences. To understand whether this variation is biologically meaningful, it is essential to discern its source. Mathematical models of biological systems are tools that can be used to investigate causes of cell-to-cell variation. From mathematical analysis and simulation of these models, biological hypotheses can be posed and investigated, then parameter inference can determine which of these is most compatible with experimental data. Data from laboratory experiments often takes the form of “snapshots” representing distributions of cellular properties at different points in times, rather than individual cell trajectories. This data is not straightforward to fit using hierarchical Bayesian methods since these approaches require inferring the identities of the groups to which individual cells belong. Here, we introduce a computational sampling method we call “Contour Monte Carlo” for estimating mathematical model parameters from snapshot distributions which is straightforward to implement and does not require assigning cells to categories *a priori*. Our method is most applicable to systems where the dominant source of uncertainty is heterogeneity in cellular processes rather than experimental measurement error which, due to the increasingly finescale resolution of laboratory techniques, may be the case for a wide class of systems. In this paper, we illustrate the use of our method by quantifying cellular variation for three biological systems of interest and provide code in the form of a Julia notebook which allows others to apply this approach to their problem.

2 Introduction

27
28
29
30
31
32
33
34
35
36
37
38
39
40
41
42
43
44
45
46
47
48
49
50

Variation, as opposed to homogeneity, is the rule rather than exception in biology. Indeed, without variation, biology as a discipline would not exist, since as evolutionary biologist JBS Haldane wrote, variation is the “raw material” of evolution. The Red Queen Hypothesis asserts that organisms must continually evolve in order to survive when pitted against other - also evolving - organisms [1]. A corollary of this hypothesis is that multicellular organisms may evolve cellular phenotypic heterogeneity to allow faster adaptation to changing environments, which may explain the observed variation in a range of biological systems [2]. Whilst cell population variation can confer evolutionary advantages, it can also be costly in other circumstances. In biotechnological processes, heterogeneity in cellular function can lead to reduced yields of biochemical products [3]. In human biology, variation across cells can enable pathologies to develop and also prevents effective medical treatment, since medical interventions typically aim to steer modal cellular properties and hence fail to influence key subpopulations. For example, cellular heterogeneity likely contributes to the persistence of some cancerous tumours [4] and may also allow them to evolve resistance to chemotherapies over time [5]. Identifying and quantifying sources of variation in populations of cells is important for a wide range of applications because it allows us to determine whether this variability is benign or alternatively requires remedy.

Mathematical models are essential tools for understanding cellular systems, whose emergent properties are the result of complex interactions

between various actors. Perhaps the simplest flavour of mathematical model used in biological systems is an ordinary differential equation (ODE) that lumps individual actors into partitions according to structure or function, and seeks to model the mean behaviour of each partition. Data from population-averaged experimental assays can be a powerful resource to understand whether such models faithfully reproduce system behaviours and can allow quantification of the interactions of various cellular components of complex metabolic, signalling and transcriptional networks. The worth of such models however is determined by whether averages mask differences in behaviour of individual cells that result in functional consequences [6]. In some cases, differences in cellular protein abundances due to biochemical “noise” may not be meaningful biologically [7] and mean cell behaviour suffices as a description of the system, whereas in others there are functional consequences. For example, a recent study demonstrated that subpopulations of clonally derived hematopoietic progenitor cells with low or high expression of a particular stem cell marker produced different blood lineages [8].

To accommodate cell population heterogeneity in mathematical models, a variety of modelling choices are available, each posing different challenges for parameter inference, and are described in a recent review [9]. These include modelling biochemical processes stochastically, with properties of ensembles of cells represented by probability distributions evolving according to chemical master equations (see [10] for a tutorial on stochastic reaction-diffusion processes; RDEs). Alternatively, population balance equations (PBEs) can be used to dictate the evolution of the “number density” of differing cell types, whose properties are represented as points in \mathbb{R}^n which, in turn, affect their function, including their rate of death and cell division (see [11] for an introduction to PBEs). In a PBE approach, variation in measured quantities results primarily due to differing functional properties of heterogeneous cell types and variable initial densities of each type.

The approach we follow here is similar to that of [12], wherein dynamic cellular variation is generated by describing the evolution of each cell’s state using an ODE, but with individual cell differences in the rate parameters of the process. To our knowledge, this flavour of model is unnamed and so, for sake of reference, we term them “heterogenous ODE” models (HODEs). In HODEs, the aim of inference is to estimate the distributions of parameter values across cells consistent with observed distributions of measurements at various timepoints. A benefit of using HODEs to model cell heterogeneity is that these models are computationally straightforward to simulate and, arguably, simpler to parameterise than PBEs. In these models the predominant source of variation is due to differences in biological processes across cells not inherent stochasticity in biochemical reactions within cells, as in stochastic RDEs.

The difficulty of parameter inference for HODEs is partly due to experimental hurdles in generating data of sufficient quality to allow identification. Unlike models which represent a population by a single scalar ODE, since HODEs are individual-based they ideally require individual cell data for estimation. A widely-used method for generating data for individual cells is flow cytometry, where a large number of cells are streamed individually through a laser beam and, for example, abundance measurements are made of proteins labelled with fluorescent markers [13]. Alternatively, experimental techniques such as Western blotting and cytometric fluorescence microscopy can generate single cell measurements [14, 15]. A property of

these experimental methods is that they are destructive, meaning that individual cells are sacrificed as part of the measurement process. This means that the measurements of cell properties obtained at a certain point in time represent what are termed “snapshots” of the underlying population [15]. These snapshots are often described by histograms [12] or density functions [9] fit to the underlying data at different points in time. Since HODEs represent the underlying state of individual cells as evolving continuously through time, corresponding data showing individual cell trajectories constitutes a richer data resource. The demands of obtaining this data are higher however and typically involve either tracking individual cells through imaging methods [16] or trapping cells in a spatial position where their individual dynamics can be readily monitored [17]. These techniques impose restrictions on experimental practices meaning they cannot be realised in all circumstances, including for online monitoring of biotechnological processes or analysis of *in vivo* studies. For this reason, snapshot data continues to play an important role for determining cell level variability in many applications.

A variety of approaches have been proposed to estimate cell-to-cell variability by fitting HODE models to snapshot data. In HODEs, parameter values vary across cells according to a to-be-determined probability distribution meaning that in order to solve the exact inverse problem, the underlying ODE system needs to be simulated for each individual. Since the numbers of cells in these experiments are typically $>\sim 10^4$ [15], this usually precludes exact inference due to its computational burden and instead the raw snapshot data is approximated by probability densities [12, 15, 18, 19]. Hasenauer et al. (2011) presents a Bayesian approach to inference for HODEs, which models the input parameter space using mixtures of ansatz densities. The authors then use their method to reproduce population substructure on synthetic data generated from a model of tumour necrosis factor stimulus. Hasenauer et al. (2014) uses mixture models to model subpopulation structure in snapshot data with multiple-start local optimisation employed to maximise the non-convex likelihood, which they then apply to synthetic and real data from signalling pathway models. Loos et al. (2018) also uses mixture models to represent subpopulation structure and a maximum likelihood approach that allows for estimation of within- and between-subpopulation variability which permits fitting to multivariate output distributions with complex correlation structures. Dixit et al. (2018) discretises cell abundances into bins, then uses a maximum entropy approach as part of a Bayesian framework to fit the distribution representing cell-to-cell variability.

The framework we present here is Bayesian although is distinct from the traditional Bayesian inferential paradigm used to fit many dynamic models since the source of stochasticity arises solely due to cell-to-cell parameter variation not measurement noise. Our approach is hence most suitable when measurement error is a minor contributor to observed experimental variability. Our computational method is a two-step Monte Carlo approach which, for reasons described in §3, we term “Contour Monte Carlo” (CMC). Unlike many of the existing methods however CMC is relatively computationally straightforward to implement and does not require extensive computation time. CMC uses MCMC in its second step to sample from the posterior distribution over parameter values and hence does not require specification of ansatz densities. It also does not require *a priori* representation of subpopulation structure using mixture components, rather,

subpopulations emerge as modes in the posterior parameter distributions.
 Like [19] CMC can fit multivariate snapshot data and unlike [12], does
 not require this data to be discretised into bins. As more experimental
 techniques are developed which elucidate single cell behaviour, there is
 likely to be more interest in methods which can be used to recapitulate
 the observed snapshots. We argue that due to its simplicity and generality,
 CMC is a useful addition to the modeller’s toolkit and can be used to
 perform inference on the proliferation of rich single cell data.

Outline of the paper: In §3, we present the details of our methodological
 framework and detail the CMC algorithm used to generate samples from
 the posterior parameter distribution. In §4, we use CMC to estimate cell
 population heterogeneity in three systems of biological interest.

3 Method

In this section, we first describe the probabilistic framework
 that underlies the CMC algorithm, before introducing CMC in pseudocode
 (Algorithm 2). We also detail the workflow we have found useful in applying
 this approach to analyse cell snapshot data and suggest practical remedies
 to issues we have encountered in using CMC (Figure 4). A glossary of all
 the variables used in this paper is included as Table 1.

Experimental methods such as flow cytometry can measure single cell
 characteristics at a given point in time. Cells are typically destroyed by
 the measurement process and so rather than providing time series for each
 individual cell, the data consists of cross-sections or “snapshots” of sampled
 individuals from the population (Figure 1).

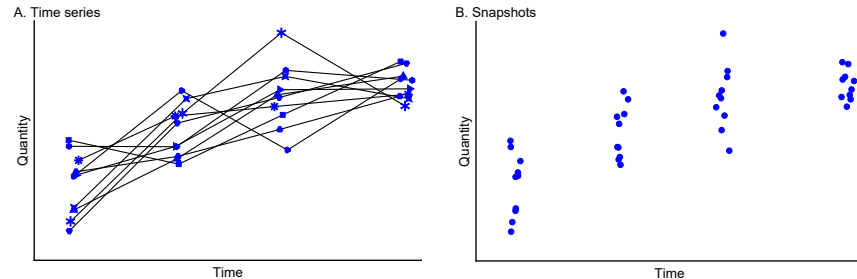


Figure 1: Time series data (A) versus snapshot data (B) typical of single cell experiments. In A that the cell identities are retained at each measurement point (indicated by given plot markers) whereas in the snapshot data in B, either this information is lost or, more often, cells are destroyed by the measurement process and so each observation corresponds to a distinct cell.

We model the processes of an individual cell using a system of ordinary
 differential equations (ODEs),

$$\begin{aligned} \frac{d\mathbf{x}}{dt} &= \mathbf{f}(\mathbf{x}(t); \boldsymbol{\theta}), \quad \mathbf{f} : \mathbb{R}^k \times \mathbb{R}^p \mapsto \mathbb{R}^k, \\ \mathbf{x}(0) &= \mathbf{x}_0 \end{aligned} \tag{1}$$

Note that in most circumstances, the initial state of the system, $\mathbf{x}(0)$,
 is unknown and it is convenient to include these as elements of $\boldsymbol{\theta}$ to be
 estimated.

In this paper, we assume variation characterised by snapshot data arises due to between-cell heterogeneity in the underlying parameters θ . Therefore, the evolution of the underlying state of cell i is described by an idiosyncratic ODE,

$$\frac{d\mathbf{x}^{\{i\}}}{dt} = \mathbf{f}(\mathbf{x}^{\{i\}}(t); \theta^{\{i\}}), \quad \mathbf{f}: \mathbb{R}^k \times \mathbb{R}^p \mapsto \mathbb{R}^k, \quad (2)$$

$$\mathbf{x}^{\{i\}}(0) = \mathbf{x}_0$$

where $\{i\}$ indicates the i th sample. The traditional (non-hierarchical) state-space approach to modelling dynamic systems supposes that measurement randomness generates output variation (Figure 2A). Our approach, by contrast, relies on the assumption that stochasticity in outputs is solely the result of variability in parameter values between cells (Figure 2B). Whether the assumption of “perfect” measurements is reasonable depends on the experimental details of the system under investigation but we argue that our method nevertheless provides a useful approximation in many cases where the signal to noise ratio is high.

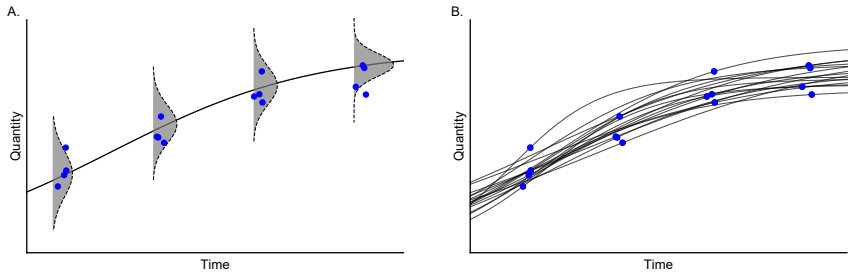


Figure 2: Two ways to generate randomness in measured outputs: the state-space model (A) versus the parameter heterogeneity model (B). For non-hierarchical state-space models (A), there is assumed to be a single “true” latent state where observations result from a noisy measurement process (grey histograms). For models with parameter heterogeneity (B), the uncertainty is generated by differences in cellular processes (black lines) between cells. Note that in both cases, individual cells are measured only once in their lifetime.

3.1 Representation of experimental data

We consider the situation in which we measure m quantities of interest $q_j, j = 1, \dots, m$.

We wish to emulate the experimental situation in which a set of observations is made. We simulate these experimental observations by solving the system of odes (1) multiple times for a range of values of parameters and calculate a (scalar-valued) quantity of interest for each value of the parameters. Let $p(\theta)$ be a probability distribution characterising heterogeneity in cellular processes and consider the situation where we have n_j observations of each quantity of interest q_j . These quantities of interest may be different functionals of the solution at the same time or the same functional at different times or a mixture of both. Define the vector containing a set of m observations as

$$\mathbf{q}^\top = (q_1, q_2, \dots, q_m) \quad (3)$$

Algorithm 1 Pseudocode for the generating raw snapshot data

```

for  $j = 1$  to  $m$  do
    for  $k = 1$  to  $n_j$  do
         $i = \sum_{l=1}^{j-1} n_l + k$ 
        Select  $\theta^{\{i\}} \sim p(\theta)$  and solve (1) for  $x^{\{i\}}(t)$ .
        Compute  $q_j(x^{\{i\}}(t_j); \theta^{\{i\}}) \in \mathbb{R}$ 
    end for
end for

```

We define

212

$$\mathbf{y}(t_j)^\top = (q_j(\tilde{x}^{\{1\}}(t_j)), q_j(\tilde{x}^{\{2\}}(t_j)), \dots, q_j(\tilde{x}^{\{n_j\}}(t_j)))^\top \in \mathbb{R}^{n_j} \quad (4)$$

and

213

$$\mathbf{X}^\top = (\mathbf{y}(t_1), \mathbf{y}(t_2), \dots, \mathbf{y}(t_m))^\top \in \mathbb{R}^s, \quad \text{where } s = \sum_{j=1}^m n_j. \quad (5)$$

The vector \mathbf{X} defines the set of experimental observations, aka, raw snapshot data.

214

Raw snapshot data thus consists of measurements of individual cells with exact inference requiring simulating the underlying ODE system for each individual cell for each quantity of interest. This is cumbersome and impractical for the numbers of cells sampled in typical experimental setups and so, instead, we follow previous work and represent snapshot data using probability distributions [12, 15, 18, 19]. These probability distributions are characterised by parameter estimates $\hat{\Phi}$ for the output vector \mathbf{Q} as determined by the output observations \mathbf{X} .

215

216

217

218

219

220

221

222

223

Variable	Definition	Dimension
$\mathbf{x}(t)$	solution of ode	\mathbb{R}^k
θ	parameters	\mathbb{R}^p
$\mathbf{f}(\mathbf{x}(t); \theta)$	RHS function of ode	\mathbb{R}^k
$\mathbf{x}^{\{i\}}(t)$	solution of ode for cell i	\mathbb{R}^k
$q_j = q_j(\mathbf{x}(t_j))$	quantity of interest (qoi) j	\mathbb{R}^1
$\mathbf{q} = (q_1, \dots, q_m)$	all m qoi	\mathbb{R}^m
$q_j^{\{i\}} = q_j(\mathbf{x}^{\{i\}}(t_j))$	quantity of interest j for cell i	\mathbb{R}^1
$\mathbf{y}_j = (q_j^{\{1\}}, \dots, q_j^{\{n_j\}})$	qoi j of cells $1, \dots, n_j$	\mathbb{R}^{n_j}
$\mathbf{X} = (\mathbf{y}_1, \dots, \mathbf{y}_m)$	system observables (all qoi)	$\mathbb{R}^s, s = \sum_{j=1}^m n_j$
Φ	parameters characterising output target distribution $p(\mathbf{q} \Phi)$	\mathbb{R}^m
Ξ	parameters characterising parameter prior distribution $p(\theta \Xi)$	\mathbb{R}^p
Ψ	parameters characterising output prior distribution $p(\mathbf{q} \Psi)$	\mathbb{R}^p
\hat{a}	estimates of any quantity a	-
$\Omega(\mathbf{z})$	region of parameter space mapping to $\mathbf{q} = \mathbf{z}$	\mathbb{R}^p
$\mathcal{V}(\mathbf{z})$	volume of parameter space mapping to $\mathbf{q} = \mathbf{z}$	\mathbb{R}^+
V	total volume of parameter space	\mathbb{R}^+

Table 1: **Glossary of variable names used in this paper.**

The goal of our inference process is to characterise the probability distribution $p(\theta|\mathbf{X})$ representing heterogeneity in cellular processes. The first step in our inference workflow is to fit the output distributions using probability distributions (Figure 4(i)). We assume that the volume

224

225

226

227

of observational data means the estimated probability distributions are approximate sufficient statistics of the outputs, meaning $p(\boldsymbol{\theta}|\hat{\Phi}) \approx p(\boldsymbol{\theta}|X)$.
228
229

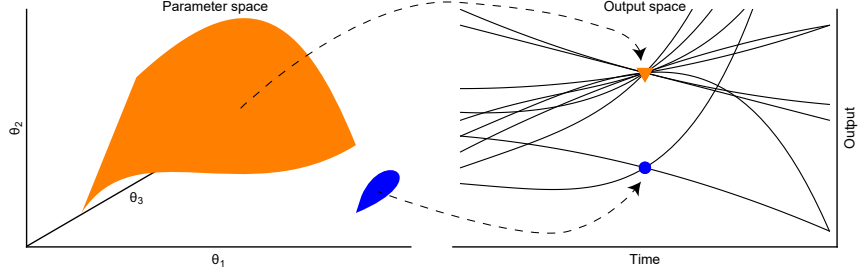


Figure 3: The non-linear mapping from parameter values (left panel) to outputs (black lines; right panel) means different sized regions of parameter space (orange and blue surfaces; left panel) correspond to distinct output values (orange triangle and blue square; right panel). In the right panel, each black line represents a distinct model simulation $g(t; \theta_1, \theta_2, \theta_3)$ and the triangle and square indicate outputs at a given point in time.
230

3.2 Theory

We consider the underdetermined case where $m < p$, so that each of the quantities of interest can be generated from a set of parameter values and any target output distribution $p(\tilde{q}|\hat{\Phi})$ does not correspond to a unique parameter distribution.
231
232
233
234

This means that in order to ensure uniqueness of the “posterior” parameter distributions, we are required to specify “prior” distributions for the parameters, as in more traditional Bayesian inference. An additional consequence of the degeneracy of the mapping from parameters to outputs is that any sampling algorithm aimed at exploring posterior parameter space must account for the differential volumes of iso-output contours. Whilst we refer the interested reader to our companion paper on this subject [citation for tutorial paper published in Open Science], we provide a quick derivation of the posterior parameter distribution which accounts for the non-linear mapping.
235
236
237
238
239
240
241
242
243
244

To derive the posterior distribution of parameter values $p(\boldsymbol{\theta}|\hat{\Phi})$, we consider the joint density of parameters and outputs $p(\boldsymbol{\theta}, (\mathbf{q}|\hat{\Phi}))$. This can be decomposed in two ways,
245
246
247

$$p(\boldsymbol{\theta}, (\mathbf{q}|\hat{\Phi})) = p(\boldsymbol{\theta}|(\mathbf{q}, \hat{\Phi})) \times p(\mathbf{q}|\hat{\Phi}) = p(\mathbf{q}|(\boldsymbol{\theta}, \hat{\Phi})) \times p(\boldsymbol{\theta}|\hat{\Phi}). \quad (6)$$

Rearranging to obtain the posterior parameter distribution,
248

$$p(\boldsymbol{\theta}|\hat{\Phi}) = \frac{p(\boldsymbol{\theta}|\mathbf{q}, \hat{\Phi}) \times p(\mathbf{q}|\hat{\Phi})}{p(\mathbf{q}|\boldsymbol{\theta}, \hat{\Phi})}. \quad (7)$$

Given parameters $\boldsymbol{\theta}$, the mapping from parameters to outputs is deterministic meaning $p(\mathbf{q}|\boldsymbol{\theta}, \hat{\Phi}) = \delta(\mathbf{q}(\boldsymbol{\theta}), \boldsymbol{\theta})$ is the Dirac delta function centred at $\mathbf{q} = \mathbf{q}(\boldsymbol{\theta})$.
249
250
251
252
253

In what follows, we assume that the conditional distribution $p(\boldsymbol{\theta}|\mathbf{q}, \hat{\Phi})$ is independent of the data, meaning it represents a conditional “prior”, which

can be manipulated by Bayes' rule,

254

$$p(\boldsymbol{\theta}|\mathbf{q}(\boldsymbol{\theta})) = \frac{p(\boldsymbol{\theta})}{p(\mathbf{q}(\boldsymbol{\theta}))}, \quad (8)$$

where we have used the Dirac delta function for $p(\mathbf{q}|\boldsymbol{\theta})$. This results in
255
the form of the posterior parameter distribution targeted by our sampling
256
algorithm,
257

$$p(\boldsymbol{\theta}|\hat{\Phi}) = \frac{p(\boldsymbol{\theta})}{p(\mathbf{q}(\boldsymbol{\theta}))} p(\mathbf{q}(\boldsymbol{\theta})|\hat{\Phi}). \quad (9)$$

Again, we refer to our companion piece [citation] for detailed explanation of
258
eqs. (8) & (9) and instead here provide brief interpretation when considering
259
a uniform prior on parameter space. In this case, $p(\boldsymbol{\theta}) = \frac{1}{V}$, where V is the
260
total volume of parameter space. The denominator term of eq. (8) is the
261
prior induced on output space by the prior over parameter space. For a
262
uniform prior on parameter values, this is
263

$$p(\boldsymbol{\theta}|\mathbf{q}(\boldsymbol{\theta})) = \frac{1}{\mathcal{V}(\mathbf{q}(\boldsymbol{\theta}))}, \quad (10)$$

where $\mathcal{V}(\mathbf{q}(\boldsymbol{\theta}))$ is the volume of parameter space occupied by the iso-output
264
region $\Omega(\tilde{\mathbf{q}}) = \{\boldsymbol{\theta} : \mathbf{q}(\boldsymbol{\theta}) = \tilde{\mathbf{q}}\}$. Therefore a uniform prior over parameter
265
space implies a prior structure where all parameter values resulting in the
266
same output $\tilde{\mathbf{q}}$ are given equal weighting.
267

3.3 Implementation

268

3.3.1 Estimation of contour volumes

269

The denominator term of eq. (8) cannot be calculated apart from for some
270
toy examples, meaning that exact sampling from the posterior parameter
271
distribution of eq. (9) is not, in general, possible. We propose instead a
272
computationally efficient sampling method to estimate $p(\mathbf{q}(\boldsymbol{\theta}))$, which forms
273
the first step of our so-called “Contour Monte Carlo” (CMC) algorithm
274
(Algorithm 2; Figure 4(ii)), where we estimate the volume of iso-output
275
contours with output value $\mathbf{q}(\boldsymbol{\theta})$. This step involves repeated independent
276
sampling from the prior distribution of parameters $\boldsymbol{\theta}^{\{i\}} \sim p(\boldsymbol{\theta}|\Xi)$, where,
277
for completeness, we have conditioned on Ξ parameterising our probability
278
density. Each parameter sample is then converted into an output value
279
 $\mathbf{q}^{\{i\}} = \mathbf{q}(\boldsymbol{\theta}^{\{i\}})$. The collection of output samples is then fitted using a
280
vine copula kernel density estimator (KDE) [20], $(\mathbf{q}^{\{1\}}, \dots, \mathbf{q}^{\{N_1\}}) \sim p(\mathbf{q}|\hat{\Psi})$.
281
Throughout the course of development of CMC, we have tested many forms
282
of KDE and have found vine copula KDE is best suited to approximating
283
the higher dimensional probability distributions required in practice.
284

3.3.2 MCMC sampling

285

The second step in our algorithm then uses Markov chain Monte Carlo
286
(MCMC) to sample from an approximate version of eq. (9) with the esti-
287
mated density $p(\mathbf{q}(\boldsymbol{\theta})|\hat{\Psi})$ replacing its corresponding estimand (Algorithm
288
2; Figure 4(iii)),
289

$$p(\boldsymbol{\theta}|\hat{\Phi}, \Xi, \hat{\Psi}) = \frac{p(\boldsymbol{\theta}|\Xi)}{p(\mathbf{q}(\boldsymbol{\theta})|\hat{\Psi})} p(\mathbf{q}(\boldsymbol{\theta})|\hat{\Phi}). \quad (11)$$

Algorithm 2 Pseudocode for the Contour Monte Carlo algorithm for sampling from the posterior parameter distribution of eq. (11). Here we provide code for the Random Walk Metropolis algorithm for the MCMC sampling but for the examples in §4, we use an adaptive MCMC algorithm [21]. A definition of all variables is provided in Table 1.

```

procedure CMC( $\mathbf{X}, \Xi, N_1, N_2$ )       $\triangleright$  Sample from posterior parameter distribution
     $\hat{\Phi} = \text{SNAPSHOTESTIMATOR}(\mathbf{X})$ 
     $\hat{\Psi} = \text{CONTOURVOLUMEESTIMATOR}(\Xi, N_1)$ 
     $(\boldsymbol{\theta}^{\{1\}}, \dots, \boldsymbol{\theta}^{\{N_2\}}) = \text{MCMC}(\hat{\Phi}, \Xi, \hat{\Psi}, N_2)$ 
    converged = COMPAREOUTPUTTOTARGET(( $\boldsymbol{\theta}_1, \dots, \boldsymbol{\theta}_{N_2}$ ),  $\hat{\Phi}$ )
    if converged ≠ 1 then           $\triangleright$  Rerun contour volume estimation and/or MCMC
        CONTOURVOLUMEESTIMATOR( $\Xi, N'_1$ ),  $N'_1 > N_1$ 
         $(\boldsymbol{\theta}^{\{1\}}, \dots, \boldsymbol{\theta}^{\{N'_2\}}) = \text{MCMC}(\hat{\Phi}, \Xi, \hat{\Psi}, N'_2)$ ,  $N'_2 > N_2$ 
         $N_1 \leftarrow N'_1$ ,  $N_2 \leftarrow N'_2$ 
    end if
    return  $(\boldsymbol{\theta}^{\{1\}}, \dots, \boldsymbol{\theta}^{\{N_2\}})$ 
end procedure

procedure SNAPSHOTESTIMATOR( $\mathbf{X}$ )            $\triangleright$  Fit density to snapshot observations
     $\mathbf{X} \sim p(\mathbf{q}|\hat{\Phi})$ 
    return  $\hat{\Phi}$ 
end procedure

procedure CONTOURVOLUMEESTIMATOR( $\Xi, N_1$ )      $\triangleright$  Estimate volume of contours
    for  $i$  in 1 :  $N_1$  do
         $\boldsymbol{\theta}^{\{i\}} \sim p(\boldsymbol{\theta}|\Xi)$            $\triangleright$  Sample from prior density
         $\mathbf{q}^{\{i\}} = \mathbf{q}(\boldsymbol{\theta}^{\{i\}})$            $\triangleright$  Calculate corresponding output value
    end for
     $(\mathbf{q}^{\{1\}}, \dots, \mathbf{q}^{\{N_1\}}) \sim p(\tilde{\mathbf{q}}|\hat{\Psi})$        $\triangleright$  Fit vine copula kernel density estimator
    return  $\hat{\Psi}$ 
end procedure

procedure MCMC( $\hat{\Phi}, \Xi, \hat{\Psi}, N_2$ )       $\triangleright$  Random Walk Metropolis algorithm targeting
posterior parameter distribution.
     $\boldsymbol{\theta}^{\{0\}} \sim \pi(\cdot)$            $\triangleright$  Sample from arbitrary initialisation distribution
    for  $i$  in 1 :  $N_2$  do
         $\boldsymbol{\theta}^{\{i'\}} \sim \mathcal{N}(\boldsymbol{\theta}^{\{i-1\}}, \Sigma)$        $\triangleright$  Propose new parameter values for parameters
         $r = \frac{[p(\boldsymbol{\theta}^{\{i'\}}|\Xi) p(\mathbf{q}(\boldsymbol{\theta}^{\{i\}})|\hat{\Psi}) p(\mathbf{q}(\boldsymbol{\theta}^{\{i'\}})|\hat{\Phi})]}{[p(\boldsymbol{\theta}^{\{i\}}|\Xi) p(\mathbf{q}(\boldsymbol{\theta}^{\{i\}})|\hat{\Psi}) p(\mathbf{q}(\boldsymbol{\theta}^{\{i\}})|\hat{\Phi})]}$ 
     $\triangleright$  Metropolis acceptance ratio.
         $u \sim U(0, 1)$            $\triangleright$  Sample from uniform distribution
        if  $r > u$  then
             $\boldsymbol{\theta}^{\{i\}} = \boldsymbol{\theta}^{\{i'\}}$            $\triangleright$  Accept proposal
        else
             $\boldsymbol{\theta}^{\{i\}} = \boldsymbol{\theta}^{\{i-1\}}$            $\triangleright$  Reject proposal
        end if
    end for
    return  $(\boldsymbol{\theta}^{\{1\}}, \dots, \boldsymbol{\theta}^{\{N_2\}})$ 
end procedure

procedure COMPAREOUTPUTTOTARGET(( $\boldsymbol{\theta}_1, \dots, \boldsymbol{\theta}_{N_2}$ ),  $\hat{\Phi}$ ) $\triangleright$  Check output distribution
close to target
    for  $i$  in 1 :  $N_2$  do
         $\tilde{\mathbf{q}}_i = \mathbf{q}(\boldsymbol{\theta}_i)$            $\triangleright$  Compute output for each parameter sample
    end for
    if  $(\tilde{\mathbf{q}}_1, \dots, \tilde{\mathbf{q}}_{N_2}) \sim p(\tilde{\mathbf{q}}|\hat{\Phi})$ ? then
        return 1           $\triangleright$  Compare outputs with target
    else
        return 0           $\triangleright$  If outputs sufficiently close then converged
    end if
end procedure

```

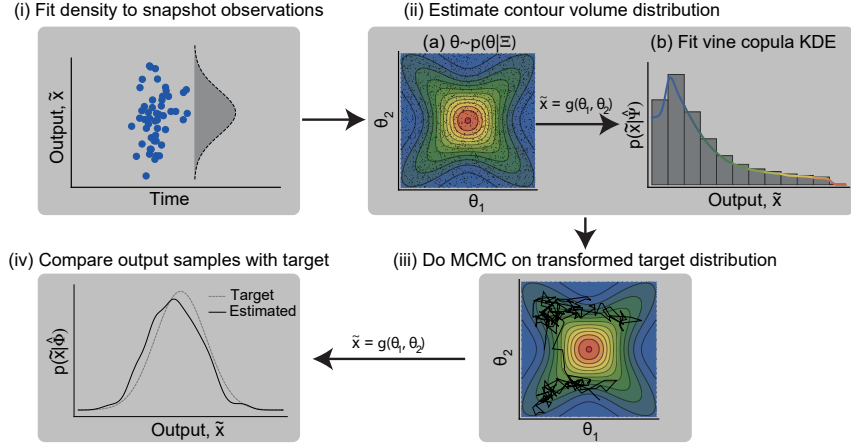


Figure 4: **The workflow for using Contour Monte Carlo to estimate cell population heterogeneity.** In (iii), the distribution targeted is given by eq. (11). The variables used in this figure are defined in the text and Table 1.

3.3.3 Reconstruction of target output distribution

The final step in CMC is to compare output samples generated from the result of the MCMC calculation with the target distribution (Figure 4(iv)). Asymptotically (in terms of the sample size of both sampling steps), CMC produces a sample of parameter values ($\theta^{\{1\}}, \theta^{\{2\}}, \dots$) which, when mapped to the output space, corresponds to the target distribution $\hat{\Psi}$. In developing CMC, we have found that a finite sample of modest size for both steps of CMC results in parameter samples that, when transformed, often represent reasonable approximations of the target. There are however occasions when this is not the case and we have found this final confirmatory step indispensable since it frequently highlights inadequacies in the contour volume estimation or the MCMC, meaning more samples from either or both of these steps are required. It may also be necessary to tweak hyperparameters of the KDE to ensure reasonable approximation in the contour volume estimation step. If the target distribution is sensitive to the contour volume estimates, this may also indicate that the target snapshot distribution is incompatible with the model: here, we make no claims on existence of a solution to the inverse problem, only that, if one should exist, Contour Monte Carlo is a pragmatic approach to approximate it by sampling. A useful way to diagnose whether the target distribution can be produced from the model and specified priors is to examine the output values from the contour volume estimation step of CMC. If the majority of probability mass of the target lies outside the bounds of the bulk simulated output values obtained by independent sampling from the prior, then the model and/or chosen prior is unlikely to be invertible to this particular target.

3.3.4 Future refinements

In generating our results in §4, for the contour volume estimation step, we assumed sample sizes were sufficient if the output samples from the MCMC provided a reasonable approximation to the target, although we recognise that future work should refine this process further. For the

MCMC step, we use adaptive covariance MCMC (see SOM of [21]) to sample from the target distribution, as we have found that it provides a considerable speed-up over Random Walk Metropolis [22, 23]. We also use the Gelman-Rubin convergence statistic \hat{R} which provides a heuristic measurement of convergence [23, 24], and use a threshold of $\hat{R} \leq \sim 1.1$ to diagnose convergence.

320
321
322
323
324
325

4 Results

326

In this section, we use CMC to estimate the posterior parameter distribution for three biological systems. We assume that the first step of CMC (“SnapshotEstimator” within Algorithm 2) has already been undertaken and we are faced with inferring a parameter distribution which, when mapped to outputs, recapitulates the target density. To accompany the text, we provide the Julia notebook used to generate the results. A table of parameters is provided in §4.4.

327
328
329
330
331
332
333

4.1 Growth factor model

334

We first consider the “growth factor model” introduced by [12], which concerns the dynamics of inactive ligand-free cell surface receptors R and active ligand-bound cell surface receptors P , modulated by an exogenous ligand L . The governing dynamics are determined by the following system,

$$\frac{dR}{dt} = R_T k_{deg} + k_1 L R(t) + k_{-1} P(t) - k_{deg} R(t) \quad (12)$$

$$\frac{dP}{dt} = k_1 L R(t) - k_{-1} P(t) - k_{deg}^* P(t), \quad (13)$$

with initial conditions

$$R(0) = ??? \quad P(0) = ???$$

where $\boldsymbol{\theta} = (R_T, k_1, k_{-1}, k_{deg}, k_{deg}^*)$ are parameters to be determined. In this example, we use measurements of the active ligand-bound receptors P to estimate cellular heterogeneity in processes. We denote the solution of eq. (13) as $P(t; \boldsymbol{\theta}, L)$ and seek to determine the parameter distribution consistent with an output distribution,

335
336
337
338
339

$$\mathbf{q} = \begin{pmatrix} q_1 \\ q_2 \end{pmatrix} = \begin{pmatrix} P(10; \boldsymbol{\theta}, 2) \\ P(10; \boldsymbol{\theta}, 10) \end{pmatrix} \sim \mathcal{N} \left[\begin{pmatrix} 2 \times 10^4 \\ 3 \times 10^4 \end{pmatrix}, \begin{pmatrix} 1 \times 10^5 & 0 \\ 0 & 1 \times 10^5 \end{pmatrix} \right]. \quad (14)$$

4.1.1 Uniform prior

340

To start, we specify a uniform prior for each of the five parameters, with bounds given in Table 3. To estimate the posterior parameter distribution, we use CMC, with adaptive covariance MCMC [21] for the second step.

In Figure 5A, we show the sampled outputs (blue points) versus the contours of the target distribution (black solid closed curves), illustrating a good correspondence between the sampled and target densities. Above and to the right of the main panel, we also display the marginal target densities (solid black lines) versus kernel density estimator reconstructions of the output marginals from the CMC samples (dashed blue lines), which again highlights the fidelity of the CMC sampled density to the target.

341
342
343
344
345
346
347
348
349
350

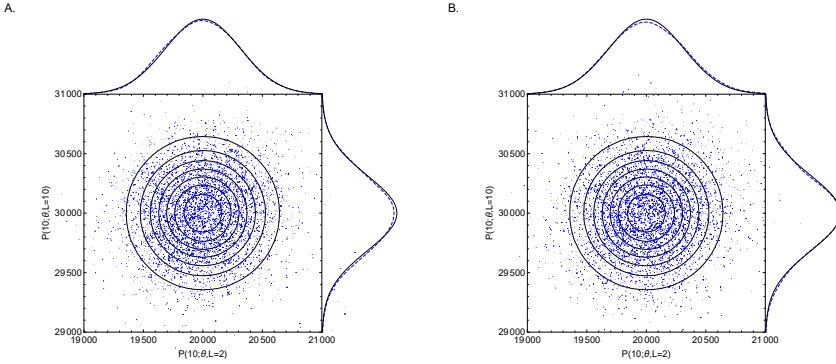


Figure 5: **The target joint output distribution (solid contour lines) and target marginal distributions (solid lines; above and to side of figure) versus outputs sampled by CMC (blue points and dashed lines) for (A) uniform and (B) normal parameter priors.** In CMC, 100,000 independent samples were used in the “ContourVolumeEstimator” step and 10,000 MCMC samples across each of 4 Markov chains were used in the second step, with the first half of the chains discarded as “warm-up” [23]. For the reconstructed marginal densities in the plots, we use Mathematica’s “SmoothKernelDistribution” function specifying bandwidths of 100 with Gaussian kernels [25].

In Figure 6A, we plot the joint posterior parameter distribution for k_1 , the rate of ligand binding to inactive receptors, and k_{-1} , which dictates the rate of the reverse reaction, where the ligands unbind. The output measurements we used to fit the model correspond to levels of the bound ligands, which can be generated whenever the ratio of k_1 to k_{-1} is approximately given by the corresponding steady state ratio. Because of this, the distribution representing cell process heterogeneity contains linear positive correlations between these parameters. In Figure 6B, we show the posterior parameter distribution for k_{deg} , the rate of degradation of ligand-free cell surface receptors and R_T , which dictates the rate of introduction of ligand-free cell surface receptors, which shows a concentrated region of posterior probability mass. Why is it that we are better able to resolve (k_{deg}, R_T) compared to (k_1, k_{-1}) from our measurements? To answer this, it is useful to calculate the sensitivity of $P(t; \theta, L)$ to changes in each of the parameters. To account for the differing magnitudes of each parameter, we calculate elasticities, the proportional changes in measured output for a proportional change in parameter values, using the forward sensitivities method described in [26], which are shown in Figure 7. When the exogenous ligand is set $L = 2$, these indicate the active ligand-bound receptor concentration is most elastic to changes in R_T and k_{deg} , meaning that their range is more restricted by the output measurement than for k_1 and k_{-1} , which have elasticities at $t = 10$ closer to 0. In Table 2, we show the posterior quantiles for the estimated parameters and, in the last column, indicate the ratio of the 25%-75% posterior interval widths to the uniform prior range for each parameter. These were strongly negatively correlated with the magnitude of the elasticities for each parameter ($\rho = 0.95$, $t = -5.22$, $df = 3$, $p = 0.01$ Pearson’s product-moment correlation), indicating the utility of sensitivity

351
352
353
354
355
356
357
358
359
360
361
362
363
364
365
366
367
368
369
370
371
372
373
374
375
376
377

analyses for optimal experimental design. We would suggest however that CMC can also be used for this purpose, using synthetic data in place of real measurements.

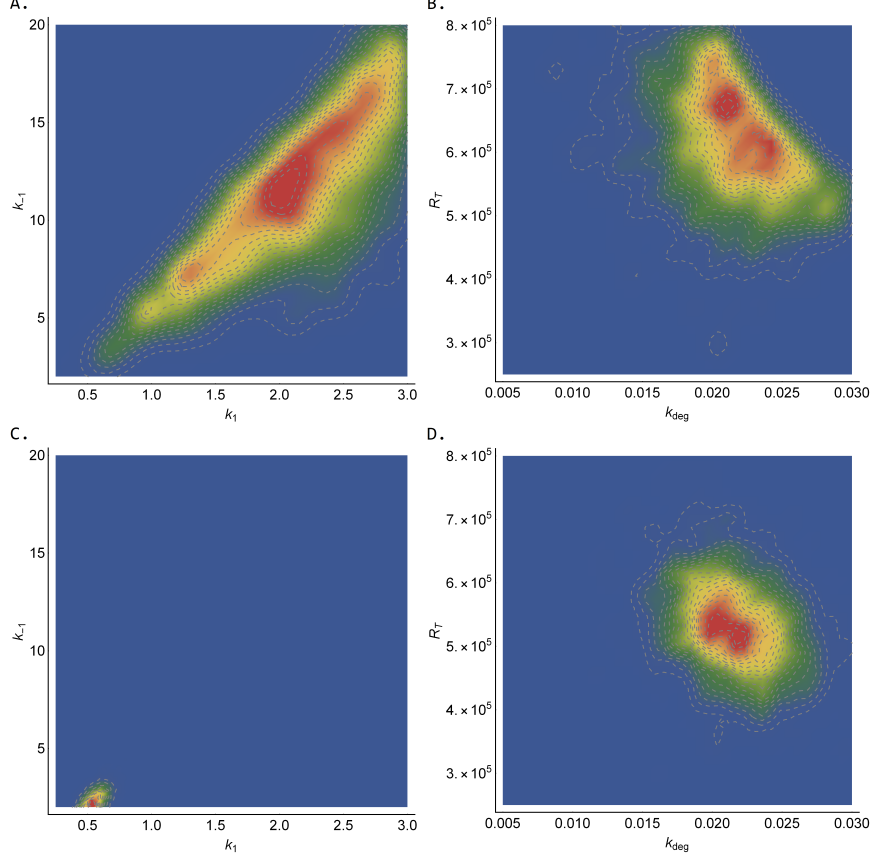


Figure 6: **The joint distributions of (k_1, k_{-1}) (left-column) and (k_{deg}, R_T) for the growth factor model using uniform priors (top row) and normal priors (bottom row).** See Figure 5 caption for CMC details and Table 3 for the priors used.

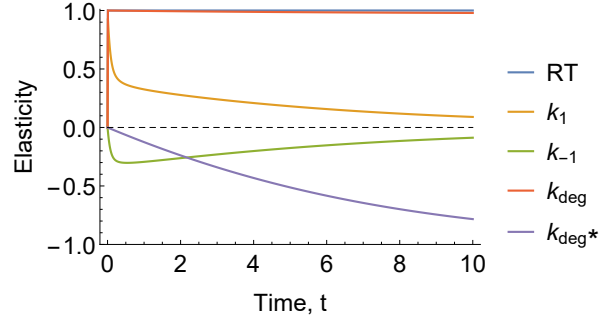


Figure 7: **The elasticities of the measured concentration of active ligand-bound receptors P versus time when $L = 2$.** When calculating the elasticities of each parameter, the other parameters were set to their posterior medians given in Table 2.

Prior	Parameter	2.5%	25%	Quantiles 50%	75%	97.5%	Posterior 25%-75% concentration
Uniform	R_T	441,006	548,275	606,439	677,055	772,484	23%
	k_1	0.90	1.69	2.17	2.56	2.95	32%
	k_{-1}	4.35	8.35	11.23	14.23	18.71	33%
	k_{deg}	0.013	0.019	0.021	0.024	0.029	20%
	k_{deg}^*	0.20	0.34	0.40	0.44	0.49	27%
Normal	R_T	408,396	487,372	529,558	577,970	678,632	16%
	k_1	0.39	0.49	0.54	0.60	0.70	4%
	k_{-1}	1.39	1.92	2.26	2.63	3.35	4%
	k_{deg}	0.016	0.020	0.022	0.024	0.027	16%
	k_{deg}^*	0.22	0.29	0.33	0.38	0.46	21%

Table 2: **Estimated quantiles from CMC samples for the growth factor model with uniform and normal priors.** The last column indicates the proportion of the uniform prior bounds occupied by the 25%-75% posterior interval in each case. The particular priors used in each case are given in Table 3.

4.1.2 Specified prior

For an unidentified model, there is typically a multitude of possible probability distributions over parameters which map to the same target output distribution. To reduce the space of posterior parameter distributions to one, it is therefore necessary to specify a prior parameter distribution. It is also preferable to allow priors to influence estimates in studies of cellular heterogeneity, since this allows incorporation of pre-existing biological knowledge with compensatory reductions in estimator variance. CMC accommodates different prior choices, with both the “ContourVolumeEstimation” step and the acceptance ratio in the “MCMC” step (Algorithm 2) being affected in such a way that posterior parameter distribution maps to the same output target. We now use CMC to estimate the posterior parameter distribution when changing from uniform priors to more concentrated normal priors (prior hyperparameters shown in Table 3). As desired, the target output distribution appears invariant (Figure 5B) although with substantial changes in the posterior parameter distributions (Figure 6C&D). In particular, the posterior distributions obtained from shifting to the normal prior are more concentrated in parameter space compared to the uniform case (rightmost column of Table 2). The differences in posterior distribution resultant from changes to priors are likely to be more marked the less definitive a guide the data provides on the underlying process and, hence, can be used to stabilise the resultant inferences according to external knowledge about the system.

4.2 Michaelis-Menten kinetics

In this section, we use CMC to invert output measurements from the Michaelis-Menten model of enzyme kinetics (see, for example, [27]); illustrating the capability of CMC to resolve population substructure from multimodality of the output distribution. The Michaelis-Menten model of enzyme kinetics describes the dynamics of concentrations of an enzyme (E), a substrate (S), an enzyme-substrate complex (ES), and a product (P).

Specifically,

$$\begin{aligned}\frac{dE}{dt} &= -k_f E(t)S(t) + k_r C(t) + k_{cat}C(t), \\ \frac{dS}{dt} &= -k_f E(t)S(t) + k_r C(t), \\ \frac{dC}{dt} &= k_f E(t)S(t) - k_r C(t) - k_{cat}C(t), \\ \frac{dP}{dt} &= k_{cat}C(t),\end{aligned}\tag{15}$$

with initial conditions,

$$E(0) = E_0, S(0) = S_0, C(0) = C_0, P(0) = P_0,\tag{16}$$

where k_f is the rate constant for the forward reaction $E + S \rightarrow C$, k_r is the rate of the reverse reaction $C \rightarrow E + S$, and k_{cat} is the catalytic rate at which the product is formed by the reaction $C \rightarrow E + P$.

When subpopulations of cells, each with distinct dynamics, are thought to exist, determining their characteristics - proportions of overall cell number, likely parameter values, and so on - is often of key interest [15, 19]. Before formal inference occurs, multi-modality of the output distribution may signal the existence of fragmented subpopulations of cells. Here we target the following bimodal bivariate normal distribution,

$$\mathbf{q} = \begin{pmatrix} q_1 \\ q_2 \end{pmatrix} = \begin{pmatrix} E(2; \boldsymbol{\theta}) \\ S(1; \boldsymbol{\theta}) \end{pmatrix} \sim \Phi(\mathbf{q}; \boldsymbol{\mu}_1, \Sigma_1, \boldsymbol{\mu}_2, \Sigma_2)\tag{17}$$

$$= \frac{1}{2} (\mathcal{N}(\mathbf{q}; \boldsymbol{\mu}_1, \Sigma_1) + \mathcal{N}(\mathbf{q}; \boldsymbol{\mu}_2, \Sigma_2)),\tag{18}$$

where $\boldsymbol{\theta} = (k_f, k_r, k_{cat})$. The parameters of the mixture normal output distribution we target are

$$\begin{aligned}\boldsymbol{\mu}_1 &= [2.2, 1.6]', \quad \Sigma_1 = \begin{pmatrix} 0.018 & -0.013 \\ -0.013 & 0.010 \end{pmatrix}, \\ \boldsymbol{\mu}_2 &= [2.8, 1.0]', \quad \Sigma_2 = \begin{pmatrix} 0.020 & -0.010 \\ -0.010 & 0.020 \end{pmatrix}.\end{aligned}$$

In what follows, we specify uniform priors on each of the elements of $\boldsymbol{\theta}$ (see Table 3).

Using a modest number of samples in each step, CMC was able to recapitulate the output target distribution (Figure 8A). Without specifying *a priori* information on the subpopulations of cells, two distinct clusters of cells emerged from application of CMC (orange and blue points in Figure 8B), each corresponding to distinct modes of the output distribution (corresponding coloured points in Figure 8A). It is worth noting however that the issues inherent with MCMC sampling of multimodal distributions similarly apply here and so, whilst here adaptive MCMC [21] sufficed to explore the posterior surface, it may be necessary to use MCMC methods known to be robust to such geometries (for example, population MCMC [28]).

411

412

413

414

415

416

417

418

419

420

421

422

423

424

425

426

427

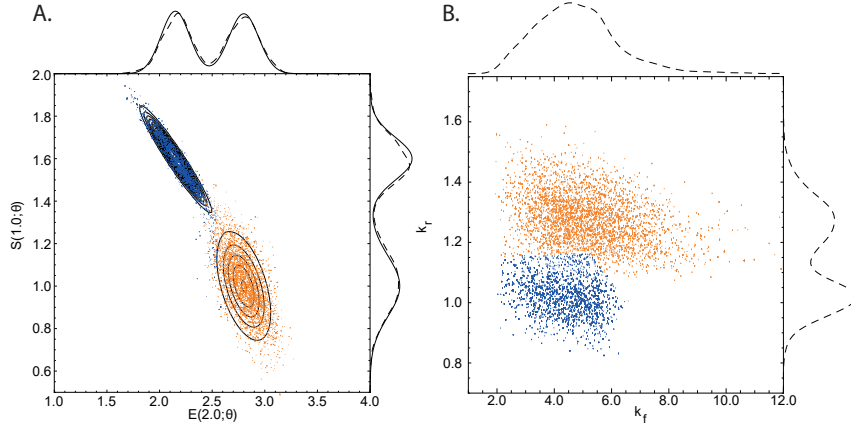


Figure 8: **(A) bimodal target distribution (solid contour lines) versus output samples (points) for the Michaelis-Menten model and (B) posterior parameter samples (points).** The solid and dashed lines above and to the side of panel A indicate the target and estimated marginal output distributions, respectively. The orange (blue) points in A were generated by the orange (blue) parameter samples in B. See Figure 5 caption for CMC details. For the reconstructed marginal densities in the plots, we use Mathematica’s “SmoothKernelDistribution” function with Gaussian kernels with (A) default bandwidths and (B) bandwidths of 0.3 (horizontal axis) and 0.03 (vertical axis) [25]. The clusters were identified by applying Mathematica’s “ClusteringComponents” function to the pairs of parameter samples displayed in B [25].

Loos et al. (2018) consider a multidimensional output distribution, with correlations between system characteristics that evolve over time. Our approach allows arbitrary covariance structure between measurements, and to exemplify this, we now target a four-dimensional output distribution, with paired measurements of enzyme and substrate at $t = 1$ and $t = 2$,

$$\begin{aligned} \mathbf{q} &= \begin{pmatrix} q_1 \\ q_2 \\ q_3 \\ q_4 \end{pmatrix} = \begin{pmatrix} E(1.0; \boldsymbol{\theta}) \\ S(1.0; \boldsymbol{\theta}) \\ E(2.0; \boldsymbol{\theta}) \\ S(2.0; \boldsymbol{\theta}) \end{pmatrix} \\ &\sim \mathcal{N} \left[\begin{pmatrix} 0.5 \\ 2.8 \\ 0.9 \\ 1.4 \end{pmatrix}, \begin{pmatrix} 0.02 & -0.05 & 0.04 & -0.05 \\ -0.05 & 0.30 & -0.15 & 0.20 \\ 0.04 & -0.15 & 0.12 & -0.17 \\ -0.05 & 0.20 & -0.17 & 0.30 \end{pmatrix} \right]. \end{aligned} \quad (19)$$

Since this system has four output measurements, and the Michaelis-Menten model has three rate parameters (k_f, k_r, k_{cat}), the system is over-identified and so CMC cannot be straightforwardly applied. Instead, we allow the four initial states (E_0, S_0, ES_0, P_0) to be uncertain quantities, bringing the total number of parameters to 7, and ensuring that the system is in the unidentified regime where CMC applies. We set uniform priors on all parameters (see Table 3) and to check that the model and priors were consistent with the output distribution given by eq. (19), we plotted the output measurements used to estimate contour volumes (in the first step of the “ContourVolumeEstimator” method in Algorithm 2) against the target (Figure 9). Since the main support of the densities (black contours) lies

429
430
431
432
433

434
435
436
437
438
439
440
441
442
443
444

within a region of output space reached by independent sampling of the priors (blue points), this indicated that the distribution given by eq. (19) could feasibly be generated from this model and priors, and we proceeded to estimation by CMC.

445
446
447
448

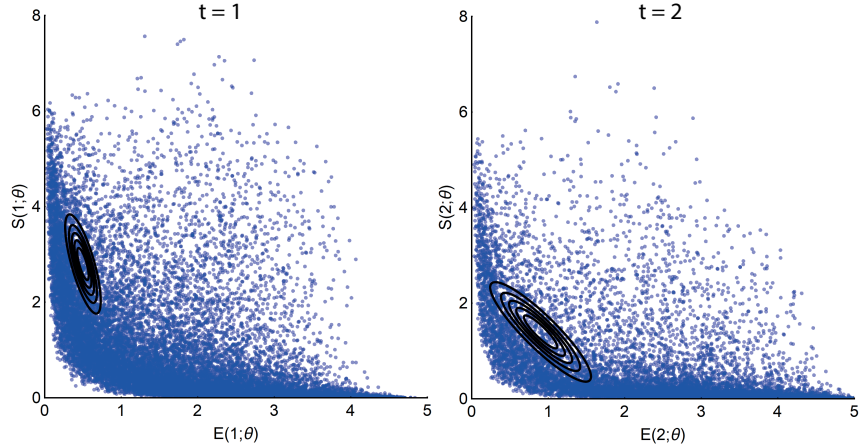


Figure 9: **The output measurements (blue points) of enzyme and substrate at times $t = 1$ (left panel) and $t = 2$ (right panel) obtained by independently sampling the priors of the 7 parameter Michaelis-Menten model versus the target distribution (black solid contours).** In this plot, we show 20,000 output samples, where each set of four measurements was obtained from a single sample of the 7 parameters. The output target distribution shown by the contours corresponds to the marginal densities of each pair of enzyme-substrate measurements given by eq. (19).

Figure 10 plots the output samples of enzyme and substrate from the last step of CMC for $t = 1$ (blue points) and $t = 2$ (orange points) versus the contours (black lines) of the joint marginal distributions of eq. (19). The distribution of paired enzyme-substrate samples illustrates that the CMC output samples approximated the target density, itself representing dynamic evolution of the covariance between enzyme and substrate measurements. The target marginal distributions (solid lines) along with their approximations from kernel density estimation (dashed lines) are also shown above and beside the main panel of Figure 10, and largely indicate correspondence.

449
450
451
452
453
454
455
456
457
458

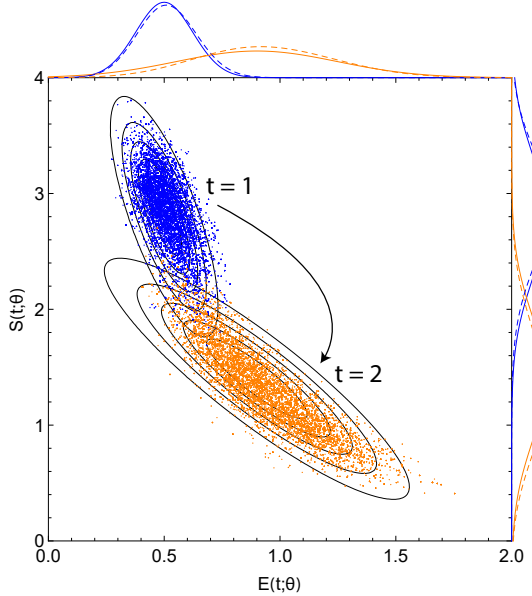


Figure 10: **Posterior output samples from CMC (coloured points) versus the contour plots of the joint marginal distributions of eq. (19) (black solid lines).** The blue and orange points indicate output observations of enzyme (horizontal axis) and substrate (vertical axis) at times $t = 1$ and $t = 2$ respectively. The solid and dashed coloured lines outside of the panels indicate the true target marginals of eq. (19) and those estimated from CMC, respectively. The line colours correspond with the point colours and indicate the marginals for $t = 1$ (blue) and $t = 2$ (orange). In CMC, 200,000 independent samples were used in the “ContourVolumeEstimator” step and 10,000 MCMC samples across each of 4 Markov chains were used in the second step, with the first half of the chains discarded as “warm-up” [23]. For the reconstructed marginal densities in the plots, we use Mathematica’s “SmoothKernelDistribution” function with Gaussian kernels [25] of bandwidths varying from 0.1 to 0.4.

4.3 TNF signalling pathway

We now illustrate how CMC can be applied to an ODE system of larger size, the tumour necrosis factor (TNF) signalling pathway model introduced in [29] and used by [15] to illustrate a Bayesian approach to cell population variability estimation. The model incorporates known activating and inhibitory interactions between four key species within the TNF pathway: active caspase 8 (x_1) and active caspase 3 (x_2), a nuclear transcription factor (x_3) and its inhibitor (x_4),

$$\begin{aligned} \frac{dx_1}{dt} &= -x_1(t) + \frac{1}{2} (\beta_4(x_3(t))\alpha_1(u(t)) + \alpha_3(x_2(t))) \\ \frac{dx_2}{dt} &= -x_2(t) + \alpha_2(x_1(t))\beta_3(x_3(t)) \\ \frac{dx_3}{dt} &= -x_3(t) + \beta_2(x_2(t))\beta_5(x_4(t)) \\ \frac{dx_4}{dt} &= -x_4(t) + \frac{1}{2} (\beta_1(u(t)) + \alpha_4(x_3(t))), \end{aligned} \quad (20)$$

459
460
461
462
463
464
465
466

with initial conditions

467

$$x_1(0) = 0.0, \quad x_2(0) = 0.0, \quad x_3(0) = 0.29, \quad x_4(0) = 0.625, \quad (21)$$

which correspond to the steady state of the system when $x_2 = 0$. The functions α_i and β_j represent activating and inhibitory interactions respectively,

$$\begin{aligned} \alpha_i(z) &= \frac{z^2}{a_i^2 + z^2}, \quad i = 1, \dots, 4, \\ \beta_j(z) &= \frac{b_j^2}{b_j^2 + z^2}, \quad j = 1, \dots, 5, \end{aligned} \quad (22)$$

and the parameters a_i for $i \in (1, 2, 3, 4)$ and b_j for $j \in (1, 2, 3, 4, 5)$ represent activation and inhibition thresholds. The function $u(t)$ represents a TNF stimulus which is given by a top hat function,

$$u(t) = \begin{cases} 1, & \text{if } t \in [0, 2], \\ 0, & \text{otherwise.} \end{cases} \quad (23)$$

When there are fewer output measurements than parameters, models tend to be underdetermined meaning that many combinations of parameters can lead to the same combination of output values. A consequence of this unidentifiability is that we cannot perform “full circle” inference: that is, using a known parameter distribution to generate an output distribution does not result in that parameter distribution being recapitulated through inference. We illustrate this idea by generating an output distribution by varying a single parameter value between runs of the forward model corresponding to the solution of eq. (20) and performing inference on all nine system parameters, whilst collecting only two output measurements. Specifically, we vary $a_1 \sim \mathcal{N}(0.6, 0.05)$, whilst holding the other parameters constant

$$(a_2, a_3, a_4, b_1, b_2, b_3, b_4, b_5) = (0.2, 0.2, 0.5, 0.4, 0.7, 0.3, 0.5, 0.4)$$

and measure $q_1 = x_1(2.0)$ and $q_2 = x_2(1.0)$. By solving the forward model using Algorithm 3.1, we obtain an output distribution that is well approximated by the bivariate normal distribution,

$$\begin{aligned} \mathbf{q} &= \begin{pmatrix} q_1 \\ q_2 \end{pmatrix} = \begin{pmatrix} x_1(2.0) \\ x_2(1.0) \end{pmatrix} \\ &\sim \mathcal{N} \left[\begin{pmatrix} 0.26 \\ 0.07 \end{pmatrix}, \begin{pmatrix} 2.1 \times 10^{-4} & 5.9 \times 10^{-5} \\ 5.9 \times 10^{-5} & 1.8 \times 10^{-5} \end{pmatrix} \right]. \end{aligned} \quad (24)$$

We now apply CMC to the target output distribution given by eq. (24) to estimate a posterior distribution over all nine parameters of eq. (20). Apart from a few cases, the priors for each parameter were chosen to *exclude* the values that were used to generate the output distribution (see Table 3), to illustrate the non-equivalence between the recovered posterior distribution and the data generating process. In Figure 11A, we plot the actual parameter values (horizontal axis) used in the true data generating process versus the inferred values (vertical axis). This illustrates that apart from a_1 , where the estimated parameter values correspond well with the range of values used to generate the data, due to the choice of priors there is a disjunction between the actual and estimated values. Despite these

468

469

470

471

472

473

474

475

476

477

478

479

480

481

482

483

484

485

486

differences, due to the model being underdetermined, it is nonetheless possible to use CMC to sample from an output distribution that well approximates the target (Figure 11B). 487
488
489

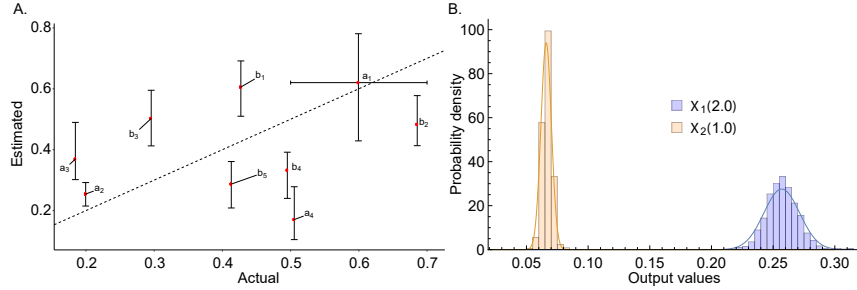


Figure 11: (A) actual parameter values versus estimated quantiles for the output distribution for the TNF signalling pathway model with output distribution given and (B) the marginal output target (solid lines) given by eq. (24) and sampled output distribution (histograms). In A, in the vertical direction, the red points indicate the 50% posterior quantiles and the upper and lower whiskers indicate the 97.5% and 2.5% quantiles, respectively; in the horizontal direction, with the exception of a_1 , the red points indicate the parameter values used to generate the data; for a_1 the red point indicates the mean of the normal distribution used to generate the data and the whiskers indicate the 95% quantiles of this distribution. In CMC, 10,000 independent samples were used in the ‘ContourVolumeEstimator’ step and 5,000 MCMC samples across each of 4 Markov chains were used in the second step, with the first half of the chains discarded as ‘warm-up’ [23]. 490
491
492
493
494
495

Cell populations may be well described by subpopulations which each evolve along characteristic trajectories over time. We now apply CMC to investigate a bimodal output distribution for the TNF signalling pathway model similar to that investigated by [15]. In particular, we aim to find a distribution over parameter values which, when used as inputs to the solution to the ODE system, results in the following output distribution, 496

$$\mathbf{q} = \begin{pmatrix} q_1 \\ q_2 \\ q_3 \end{pmatrix} \quad (25)$$

where 497

$$\begin{aligned} q_1 &= \mathbf{x}_2(1.0) \sim \mathcal{N}(0.06, 0.01) \\ q_2 &= \mathbf{x}_2(2.0) \sim \frac{1}{2} (\mathcal{N}(0.1, 0.01) + \mathcal{N}(0.14, 0.01)) \\ q_3 &= \mathbf{x}_2(4.0) \sim \frac{1}{2} (\mathcal{N}(0.1, 0.01) + \mathcal{N}(0.20, 0.01)), \end{aligned} \quad (26) \span style="float: right;">498
499
500
501
502
503$$

where the target distributions for $\mathbf{q}_2(2.0)$ and $\mathbf{q}_2(4.0)$ indicate mixtures of univariate normals, and the priors used are shown in Table 3. This target distribution, along with the unique trajectories obtained by applying the CMC algorithm for 5,000 MCMC steps, are shown in Figure 12. This figure illustrates that given by bimodality of the output distribution, CMC estimates a corresponding subpopulation structure in the parameter distribution without *a priori* specification of the number of clusters. 504

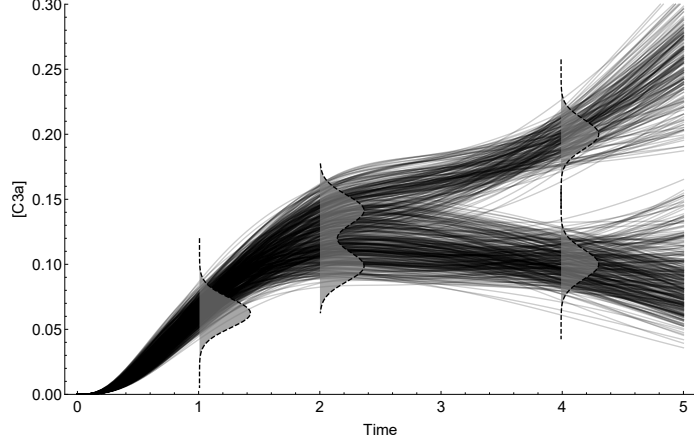


Figure 12: **The target output distribution (dashed plots with grey filling) and unique trajectories (black solid lines) obtained from the posterior parameter distribution.** In CMC, 10,000 independent samples were used in the “ContourVolumeEstimator” step and 5,000 MCMC samples across each of 4 Markov chains were used in the second step, with the first half of the chains discarded as “warm-up” [23].

4.4 Parameters

504

5 Discussion

505

Determining the cause of variability in cellular processes is crucial in many applications, ranging from bioengineering to drug development. In this paper, we introduce a Bayesian method for estimating cellular heterogeneity from “snapshot” measurements of cellular properties, taken at discrete intervals throughout the experimental course. Our approach assumes what we term a “heterogeneous ordinary differential equation” (HODE) framework, in which biochemical processes in individual cells are assumed to follow dynamics governed by a common ODE, although with idiosyncratic differences in parameter values. In this framework, estimating heterogeneity in cellular processes amounts to determining the probability distributions over parameter values of the governing ODE. Our method of estimation is a two-step Monte Carlo sampling process we term “Contour Monte Carlo” (CMC) which does not require *a priori* specification of cell population substructure unlike other approaches. CMC can be used to process high volumes of individual cellular measurements since the framework involves fitting a kernel density estimator to raw experimental data and using these distributions rather than data as the target outcome. CMC also allows for arbitrary multivariate structure in the measurement space, meaning it can capture correlations that occur between the same cellular species at different timepoints or, for example, contemporaneous correlations between different cellular compartments. Being a Bayesian approach, CMC uses prior distributions over parameter values to ensure uniqueness of the posterior distribution, allowing pre-experimental knowledge to be used to improve estimation robustness. The flexible and robust framework that CMC provides means it can be used to do automatic inference for wide-ranging systems of practical interest.

As well as providing a framework for estimating cellular variation,

506
507
508
509
510
511
512
513
514
515
516
517
518
519
520
521
522
523
524
525
526
527
528
529
530
531
532

Model	Target density	Parameter	Prior density	Prior p_1	Prior p_2
Growth factor	2-dimensional normal	R_T	uniform	2.5×10^5	8×10^5
		k_1	uniform	0.25	3.0
		k_{-1}	uniform	2.0	20.0
		k_{deg}	uniform	0.005	0.03
		k_{deg}^*	uniform	0.1	0.5
Growth factor	2-dimensional normal	R_T	normal	5×10^5	1×10^5
		k_1	normal	0.5	0.1
		k_{-1}	normal	3.0	1.0
		k_{deg}	normal	0.02	0.005
		k_{deg}^*	normal	0.3	0.1
Michaelis-Menten	bimodal normal	k_f	uniform	0.2	15
		k_r	uniform	0.2	2.0
		k_{cat}	uniform	0.5	3.0
Michaelis-Menten	4-dimensional normal	k_f	uniform	0.2	15
		k_r	uniform	0.2	2.0
		k_{cat}	uniform	0.2	3.0
		E_0	uniform	3.0	5.0
		S_0	uniform	5.0	10.0
		ES_0	uniform	0.0	0.2
		P_0	uniform	0.0	0.2
TNF signalling	bivariate normal	a_1	uniform	0.4	0.8
		a_2	uniform	0.1	0.7
		a_3	uniform	0.3	0.7
		a_4	uniform	0.1	0.3
		b_1	uniform	0.5	0.7
		b_2	uniform	0.4	0.6
		b_3	uniform	0.4	0.6
		b_4	uniform	0.2	0.4
		b_5	uniform	0.2	0.4
		a_1	uniform	0.5	0.7
TNF signalling	bimodal normal	a_2	uniform	0.1	0.3
		a_3	uniform	0.1	0.3
		a_4	uniform	0.4	0.6
		b_1	uniform	0.3	0.5
		b_2	uniform	0.6	0.8
		b_3	uniform	0.2	0.4
		b_4	uniform	0.4	0.6
		b_5	uniform	0.3	0.5

Table 3: The priors used for each problem in §4.

our approach also provides a natural way to test that it is working as
desired. By feeding the posterior parameter samples obtained by CMC into
the forward model, this results in a distribution over output values that
can be compared to the target. Indeed, we have found this comparison
indispensable in applying CMC in practice and include it as the last step
in the CMC algorithm (Algorithm 2). Discrepancies between the target
output distribution and samples from it by CMC can occur either as a
result of poor estimates of the “contour volume distribution” in the first
stage of the algorithm or due to insufficient MCMC samples in the second.
Either of these issues can often be easily addressed and although kernel
density estimation in high dimensional spaces remains an open research
problem, we have found vine copula kernel density estimation works well
for the dimensionality of output measurements we investigate here [20].

Failure to reproduce a given output distribution can also indicate that
the generating model (the priors and the forward model) are incongruent
with experimental results. This may either be due to misspecification of the
ODE system or the inadequacy of the assumed deterministic framework.
Our approach currently assumes that output stochasticity is dominated by
cellular variation in the parameter values of the underlying ODE, with mea-
surement noise making a minor contribution. Whether this is a reasonable
assumption depends on the system under investigation and, more impor-
tantly, on experimental details. We recognise that neglecting measurement
noise when it is an important determinant of the observed data is likely
to mean we overstate the degree of cellular variation. It may also mean
that some output distributions cannot be obtained through our assumed
model system. Future work allowing inclusion of a stochastic noise process
or, more generally, including stochastic cellular mechanisms is thus likely
to be worthwhile.

Whilst we have labelled the approach we follow here as Bayesian, since it
involves explicit estimation of probability distributions and involves priors
over parameter values, we recognise that it is not in the form typically
utilised by exponents of this framework. This is because rather than aiming
to formulate a model that describes output observations, instead, our
approach aims to recapitulate output distributions. Others [30], (including
us [31]), have considered this problem before; perhaps most notably by
Albert Tarantola in his landmark work on inverse problem theory (see,
for example, [32]). In Tarantola’s framework, a joint input parameter &
output space is considered, where prior knowledge and experimental theory
combine elegantly to produce a posterior distribution whose marginal output
distribution matches the experimentally obtained one. This work has seen
considerable interest in areas such as the geosciences [33,34], and we propose
that these methods may prove useful for the biosciences. In particular, we
posit that this framework may permit a generalised Bayesian inference that
can more parsimoniously encompass output data and output distributions
as their outcome measures.

The natural world is rife with variation. Mathematical models represent
frameworks for understanding the causes of such variation. Typically, the
state of biological knowledge is such that one effect, a given pattern of
variation, has many possible causes, and observational or experimental
data are necessary to apportion weight to each of them, in a process
which amounts to solving inverse an problem. The approach we describe
here follows the Bayesian paradigm of inverse problem solving whereby
uncertainty in potential causes is reflected by probability distributions. Here,

we illustrate the utility of our method by applying it to estimate cellular heterogeneity in biochemical processes however, it could equally well be used to understand the inversion of deterministic systems more generally. Whilst describing the inversion process of deterministic models using probability distributions may sound contradictory, it is worth acknowledging that many ODE systems are structurally unidentified meaning there is incompressible uncertainty over some regions of parameter space. Contour Monte Carlo provides an automatic framework for doing inference on these deterministic systems and the use of priors allows for robust and precise parameter estimation unattainable through the data alone. 586
587
588
589
590
591
592
593
594
595

6 Author contributions

BL, DJG and SJT conceived the study. BL carried out the analysis. All authors helped to write and edit the manuscript. 597
598

References

- [1] M Ridley. *The red queen: Sex and the evolution of human nature.* Penguin UK, 1994.
- [2] D Fraser and M Kaern. A chance at survival: gene expression noise and phenotypic diversification strategies. *Molecular Microbiology*, 71(6):1333–1340, 2009.
- [3] F Delvigne, Q Zune, AR Lara, W Al-Soud, and SJ Sørensen. Metabolic variability in bioprocessing: implications of microbial phenotypic heterogeneity. *Trends in Biotechnology*, 32(12):608–616, 2014.
- [4] RA Gatenby, K Smallbone, PK Maini, F Rose, J Averill, Raymond B Nagle, L Worrall, and RJ Gillies. Cellular adaptations to hypoxia and acidosis during somatic evolution of breast cancer. *British Journal of Cancer*, 97(5):646, 2007.
- [5] PM Altrock, LL Liu, and F Michor. The mathematics of cancer: integrating quantitative models. *Nature Reviews Cancer*, 15(12):730, 2015.
- [6] SJ Altschuler and LF Wu. Cellular heterogeneity: do differences make a difference? *Cell*, 141(4):559–563, 2010.
- [7] MB Elowitz, AJ Levine, ED Siggia, and PS Swain. Stochastic gene expression in a single cell. *Science*, 297(5584):1183–1186, 2002.
- [8] HH Chang, M Hemberg, M Barahona, DE Ingber, and S Huang. Transcriptome-wide noise controls lineage choice in mammalian progenitor cells. *Nature*, 453(7194):544, 2008.
- [9] S Waldherr. Estimation methods for heterogeneous cell population models in systems biology. *Journal of The Royal Society Interface*, 15(147):20180530, 2018.
- [10] R Erban, J Chapman, and P Maini. A practical guide to stochastic simulations of reaction-diffusion processes. *arXiv preprint arXiv:0704.1908*, 2007.

- [11] D Ramkrishna and MR Singh. Population balance modeling: current status and future prospects. *Annual Review of Chemical and Biomolecular Engineering*, 5:123–146, 2014.
- [12] P Dixit, E Lyashenko, M Niepel, and D Vitkup. Maximum entropy framework for inference of cell population heterogeneity in signaling network dynamics. *bioRxiv*, page 137513, 2018.
- [13] WG Telford, T Hawley, F Subach, V Verkhusha, and RG Hawley. Flow cytometry of fluorescent proteins. *Methods*, 57(3):318–330, 2012.
- [14] AJ Hughes, DP Spelke, Z Xu, CC Kang, DV Schaffer, and AE Herr. Single-cell western blotting. *Nature methods*, 11(7):749, 2014.
- [15] J Hasenauer, S Waldherr, M Doszczak, N Radde, P Scheurich, and F Allgöwer. Identification of models of heterogeneous cell populations from population snapshot data. *BMC Bioinformatics*, 12(1):125, 2011.
- [16] O Hilsenbeck, M Schwarzfischer, S Skylaki, B Schauberger, PS Hoppe, D Loeffler, KD Kokkaliaris, S Hastreiter, E Skylaki, A Filipczyk, et al. Software tools for single-cell tracking and quantification of cellular and molecular properties. *Nature Biotechnology*, 34(7):703, 2016.
- [17] FSO Fritzsch, C Dusny, O Frick, and A Schmid. Single-cell analysis in biotechnology, systems biology, and biocatalysis. *Annual Review of Chemical and Biomolecular Engineering*, 3:129–155, 2012.
- [18] J Hasenauer, C Hasenauer, T Hucho, and FJ Theis. ODE constrained mixture modelling: a method for unraveling subpopulation structures and dynamics. *PLOS Computational Biology*, 10(7):e1003686, 2014.
- [19] C Loos, K Moeller, F Fröhlich, T Hucho, and J Hasenauer. A hierarchical, data-driven approach to modeling single-cell populations predicts latent causes of cell-to-cell variability. *Cell Systems*, 6(5):593–603, 2018.
- [20] T Nagler and C Czado. Evading the curse of dimensionality in non-parametric density estimation with simplified vine copulas. *Journal of Multivariate Analysis*, 151:69–89, 2016.
- [21] RH Johnstone, ETY Chang, R Bardenet, TP De Boer, DJ Gavaghan, P Pathmanathan, RH Clayton, and GR Mirams. Uncertainty and variability in models of the cardiac action potential: Can we build trustworthy models? *Journal of Molecular and Cellular Cardiology*, 96:49–62, 2016.
- [22] N Metropolis, AW Rosenbluth, MN Rosenbluth, AH Teller, and E Teller. Equation of state calculations by fast computing machines. *The Journal of Chemical Physics*, 21(6):1087–1092, 1953.
- [23] B Lambert. *A Student’s Guide to Bayesian Statistics*. Sage Publications Ltd., 2018.
- [24] A Gelman and DB Rubin. Inference from iterative simulation using multiple sequences. *Statistical Science*, pages 457–472, 1992.
- [25] Inc. Wolfram Research. Mathematica 8.0. <https://www.wolfram.com>.

- [26] AC Daly, DJ Gavaghan, J Cooper, and SJ Tavener. Inference-based assessment of parameter identifiability in nonlinear biological models. *Journal of The Royal Society Interface*, 15, 2018.
- [27] JD Murray. *Mathematical biology: I. An Introduction (interdisciplinary applied mathematics)*(Pt. 1). New York, Springer, 2007.
- [28] A Jasra, DA Stephens, and CC Holmes. On population-based simulation for static inference. *Statistics and Computing*, 17(3):263–279, 2007.
- [29] M Chaves, T Eissing, and F Allgower. Bistable biological systems: A characterization through local compact input-to-state stability. *IEEE Transactions on Automatic Control*, 53(Special Issue):87–100, 2008.
- [30] T Butler, J Jakeman, and T Wildey. Combining push forward measures and baye’s rule to construct consistent solutions to stochastic inverse problems. *SIAM J. Sci. Comput.*, 40(2):A984–A1011, 2018.
- [31] B Lambert, D Gavaghan, and SJ Tavener. Inverse sensitivity analysis of mathematical models avoiding the curse of dimensionality. *BioRxiv*, page 432393, 2018.
- [32] A Tarantola. *Inverse problem theory and methods for model parameter estimation*, volume 89. SIAM, 2005.
- [33] K Mosegaard and A Tarantola. Monte Carlo sampling of solutions to inverse problems. *Journal of Geophysical Research: Solid Earth*, 100(B7):12431–12447, 1995.
- [34] T Vukicevic and D Posselt. Analysis of the impact of model nonlinearities in inverse problem solving. *Journal of the Atmospheric Sciences*, 65(9):2803–2823, 2008.